# DEFORMATION OF ODD NUCLEI $^{27}$Al, $^{31}$P AND $^{35}$Cl IN SINGLE-PARTICLE STATES[†]

**Volodymyr Yu. Korda[a,*], Larisa P. Korda[b], Vyacheslav F. Klepikov[a], Iryna S. Timchenko[b]**

*[a]Institute of Electrophysics and Radiation Technologies, National Academy of Sciences, Kharkiv 61002, Ukraine*
*[b]National Science Center "Kharkiv Institute of Physics and Technology", National Academy of Sciences, Kharkiv 61108, Ukraine*
*\*Corresponding Author e-mail: kvyu@kipt.kharkov.ua*

Using the evolutionary approach recently developed by us, the shapes of odd s-d-shell $^{27}$Al, $^{31}$P and $^{35}$Cl nuclei in the ground and single-particle excited states have been extracted from the experimental data on the energies, spins, and parities of these states, as well as the measured probabilities of electromagnetic transitions between them. The key ingredient of our procedure is the evolutionary algorithm that evolves the population of the bad-quality data-fitting nuclear shapes to the high-quality data-fitting nuclear shapes. We have found that the studied nuclei in the ground states are abnormally weakly deformed, which is not expected for the nuclei in the shell middle. Even in their low-laying single-particle excited states, the nuclei $^{27}$Al and $^{31}$P are found to be weakly deformed, too. With the increase of the single-particle excitation energy, the change of the state of the only one nucleon – the valence proton the spin and parity of which determine the spin and parity of the $^{35}$Cl nucleus – causes the shape phase transition from the high-symmetry phase – spherical ground state – to the low-symmetry phase – deformed excited states. The angular part of the $^{27}$Al and $^{31}$P nuclei shape is described by two harmonics – quadrupole and hexadecapole. The angular part of the $^{35}$Cl nucleus shape is described by three harmonics – quadrupole, hexadecapole, and hexacontatetrapole, but the contribution of hexadecapole deformation is not independent. At present, there are no fundamental nuclear models that account for or predict the dominant hexacontatetrapole deformation, especially for light and medium nuclei. We have found that the spin and parity of the $^{27}$Al, $^{31}$P and $^{35}$Cl nuclei are determined by the spin and parity of the last odd (valence) proton. At the same time, some of the nucleons of the nucleus core change their characteristics, too. Thus, the electromagnetic transitions between the single-particle states of the $^{27}$Al, $^{31}$P and $^{35}$Cl nuclei are the multi-particle processes.

**Keywords:** *Nuclear deformation; Deformed shell model; Single-particle state; s-d-shell nuclei; Evolutionary algorithm; Shape phase transition*

**PACS:** 21.60.−n, 21.60.Cs, 21.60.Ev, 27.30.+t

## 1. INTRODUCTION

Complex, multi-particle nature of nuclear forces makes nuclear physics a largely eclectic science: to understand different observable properties of nuclei, it is often necessary to use different concepts from different areas of physics (see, e.g., Refs. [1,2] or any textbook on nuclear physics). And any new idea is always welcome.

So, to understand the origin of nuclear deformation, the concept of phase transitions and the Landau theory of phase transitions, proposed and well developed for condensed matter physics [3], turned out to be useful (see, e.g., review [4] and references therein). Indeed, the very fact of the appearance of a deformation of the nucleus shape caused by a change in, say, the number of nucleons in the nucleus can be considered as a result of phase transition from a high-symmetry (spherical) phase to a low-symmetry (deformed) phase of a nucleus. Thus, spontaneous breaking of rotational symmetry of a spherical nucleus can be accepted as an origin of nuclear deformation. The Landau theory of phase transitions is well suited for describing such shape phase transitions in a phenomenological language.

Currently known applications of the Landau theory to shape phase transitions suggest that the potential energy of the nucleus (in the form of thermodynamic potentials, Helmholtz free energy, Gibbs free energy, etc.) has the form of a polynomial from rotationally invariant combinations of quadrupole deformation parameters introduced by Bohr and Mottelson [5]. Such a polynomial is either the by-product of microscopic or semi-microscopic calculations (as, e.g., in the interacting boson and boson-fermion models), or is parameterized directly (as, e.g., in geometric collective models) [4]. The coefficients of the polynomial depend on the control parameter associated with the number of nucleons in the nucleus. Equilibrium deformation parameters minimize potential energy. A change in the control parameter leads to a transition from a spherical phase, for which the equilibrium deformation parameters are zero, to deformed phases, for which the equilibrium deformation parameters differ from zero. Following this recipe, interesting data were described and phase transitions of the first and second order were identified (see, e.g., reviews [6–8] and references therein).

Presently, the dynamics of nuclear shape caused by a change in the number of nucleons in the nucleus is mainly studied (see, e.g., [4,9,10]). However, the same nucleus in different single-particle states can have different shapes too and, in principle, the shape phase transition can be caused not only by changing the number of nucleons in the nucleus, but also by changing the states of nucleons in the nucleus. Regardless of the method of calculation, the shape of the nucleus in the single-particle state strongly influences its wave function. The wave functions of the initial and final states of the nucleus largely determine the probability of electromagnetic transition between them. Therefore, the experimentally observed probabilities of electromagnetic transitions are a valuable source of information about the shape of the nucleus in various single-particle states.

The generalized nucleus model (in the form of Nilsson model [5,11]) allows, in principle, to calculate the equilibrium deformation of the nucleus in any single-particle state. In fact, Nilsson model with spin-orbit coupling describes the sequence of shape phase transitions because it predicts spherically symmetric equilibrium shape of the equipotential surface of a nucleus if all states with the shell number $N$ and the total momentum $I$ are occupied. However, the probabilities of electromagnetic transitions can only be calculated between single-particle states with the same deformation. In a number of works [12–18], the modification of Nilsson model was proposed, in which the deformation of the nucleus was considered as a dynamic parameter. That is, the initial and final states are assumed to have different deformations. Thus, during the transition, the states of all nucleons can change.

The modified Nilsson model enabled to calculate the probabilities of electromagnetic transitions between single-particle states, taking into account their different deformations [12–18]. The assumption of the dynamic nature of the deformation of single-particle states of odd s-d-shell nuclei significantly reduced the discrepancy between the measured and calculated probabilities of some $E2$-transitions. However, it appeared impossible to adequately describe the entire set of experimental data, including energies, spins and parities of the ground and single-particle excited states, as well as the probabilities of both $E$- and $M$-transitions between them.

That is why it would be highly desirable to have a procedure that could extract the angular dependence (deformation) of the potential of the self-consistent field of the nucleus in the ground and single-particle excited states directly from the experimental data on the energies, spins, and parities of the states of nuclei, as well as the measured probabilities of electromagnetic transitions between these states [19]. The goal that this procedure could be aimed at is the study of the shape of odd s-d-shell nuclei, both in the ground and low-laying single-particle excited states and the search for possible phase transitions from spherical to deformed states of the nucleus.

## 2. DEFORMED-SHELL-MODEL SINGLE-PARTICLE HAMILTONIAN

We restrict ourselves to the case of an axially symmetric nucleus with an additional symmetry plane perpendicular to the symmetry axis. We chose a single-particle harmonic-oscillator potential with the spin-orbit interaction (see, e.g., Refs. [5,11]). Making a direct generalization, we write the single-particle Hamiltonian in the form:

$$H = \hbar\omega(H_0 + H_1), \quad H_0 = \left(-\Delta + r^2\right)/2, \quad H_1 = -r^2\varphi(\theta)/2 - 2\kappa(\mathbf{l}\cdot\mathbf{s})[1 - \varphi(\theta)], \tag{1}$$

where $r$ is the reduced coordinate; $1/\sqrt{1-\varphi(\theta)}$ is the reduced radius of the equipotential surface of the nuclear potential; $\theta$ is the polar angle, $\theta \in [0; \pi/2]$; $\varphi(\theta)$ is the function that describes the shape of the equipotential surface, $\varphi(\pi - \theta) \equiv \varphi(\theta)$, $d\varphi/d\theta \equiv 0$ at the points $\theta = 0$ and $\theta = \pi/2$; $r^2\varphi(\theta)$ is the coupling of the particle with the symmetry axis; $(\mathbf{l}\cdot\mathbf{s})$ is the spin-orbit interaction; $(\mathbf{l}\cdot\mathbf{s})\varphi(\theta)$ is the coupling of the spin-orbit interaction with the symmetry axis; $\hbar\omega = 41A^{-1/3}(1 + \varepsilon)$ MeV is the energy scale; $A = N + Z$ is the nucleus mass number; $N$ and $Z$ are the numbers of neutrons and protons in the nucleus; $\varepsilon$ takes into account the deviation of the energy scale from its simple estimate. We do not expect the nucleus volume to conserve because we are aimed at extracting the nucleus shape (including its radius) directly from the available data.

In our approach, by definition, the function $\varphi(\theta)$ contains all information on the nuclear shape. Initially, no deformation parameters are needed to determine it. The function $\varphi(\theta)$ directly and explicitly enters in the total Hamiltonian $H$ (1) (generally, as a numerical array). Using as a basis the eigenfunctions of the spherical harmonic oscillator Hamiltonian $H_0$ from Eq. (1), the matrix of the total Hamiltonian $H$ is numerically diagonalized (see Ref. [11] for details). As a result, the eigenfunctions of the Hamiltonian $H$ appear as a finite mixture of the eigenfunctions of the Hamiltonian $H_0$. The coefficients of the mixture are calculated numerically and, in this way, contain information on the nuclear shape. The single-particle wave function of the nucleus in a certain state is the Slater determinant constructed from the occupied single-particle states calculated using the Hamiltonian $H$ (1). We emphasize that this wave function directly and explicitly depends on the mixture coefficients but not on any deformation parameters.

## 3. PROBABILITIES OF ELECTROMAGNETIC TRANSITIONS BETWEEN SINGLE-PARTICLE STATES WITH DIFFERENT DEFORMATIONS

To determine the matrix element of the single-particle multipole operator

$$\mathsf{M} = \sum_{s=1}^{A} \hat{t}_s, \tag{2}$$

we consider two sets of occupied single-particle states

$$\begin{aligned}
\{u_j\}, j = 1, \ldots, N, N+1, \ldots, N+Z \\
\{v_i\}, i = 1, \ldots, N, N+1, \ldots, N+Z
\end{aligned}, \tag{3}$$

calculated using the Hamiltonian (1) with two different functions $\varphi(\theta)$, which form two Slater determinants $\Psi\{u_j\}$ and $\Psi'\{v_i\}$. The matrix element of M, taken between $\Psi\{u_j\}$ and $\Psi'\{v_i\}$, is equal to (see, e.g., [20])

$$(\Psi', M\Psi) = \sum_{s=1}^{A} |\mathbf{M}^s|, \tag{4}$$

where the elements of determinants $|\mathbf{M}^s|$ are as follows

$$\mathbf{M}_{ij}^s = \begin{cases} (v_i, \hat{t}_s u_j), & i = s, \\ (v_i, \quad u_j), & i \neq s. \end{cases} \tag{5}$$

The reduced electric and magnetic multipole transition probabilities between the initial and final states with $IK$ and $I'K'$, where $I$ and $K$ are the total momentum and its projection take the form ($\lambda < K + K'$) [12–14]:

$$B(E\lambda; IK \to I'K') = e^2 \left[ 1 + (-1)^\lambda \frac{Z}{A^\lambda} \right] \left( \frac{\hbar}{m\omega} \right)^\lambda \frac{2\lambda+1}{4\pi} \left| \langle I\lambda KK' - K \mid I'K' \rangle \right|^2 \left| \mathbf{N} \right| \sum_{s=N+1}^{N+Z} \left| \mathbf{z}_E^s \right| \Big|^2 \tag{6}$$

$$B(M\lambda; IK \to I'K') = \left( \frac{e\hbar}{2mc} \right)^2 \left( \frac{\hbar}{m\omega} \right)^{\lambda-1} \frac{2\lambda+1}{16\pi} \left| \langle I\lambda KK' - K \mid I'K' \rangle \right|^2 \left| \mathbf{z} \right| \sum_{s=1}^{N} \left| \mathbf{N}^s \right| + \left| \mathbf{N} \right| \sum_{s=N+1}^{N+Z} \left| \mathbf{z}_M^s \right| \Big|^2 \tag{7}$$

$$\mathbf{N}_{ij} = (v_i, u_j) = \delta_{N_i N_j} \sum_{l\Lambda} a_{l\Lambda}^i a_{l\Lambda}^j, \quad \mathbf{N}_{ij}^s = \begin{cases} G_{M\lambda}^{ij}, & i = s, \\ \mathbf{N}_{ij}, & i \neq s, \end{cases} i, j = 1, \ldots, \tag{8}$$

$$\mathbf{Z}_{ij} = (v_i, u_j) = \delta_{N_i N_j} \sum_{l\Lambda} a_{l\Lambda}^i a_{l\Lambda}^j, \quad \mathbf{z}_{E(M)ij}^s = \begin{cases} G_{E(M)\lambda}^{ij}, & i = s, \\ \mathbf{Z}_{ij}, & i \neq s, \end{cases} i, j = N+1, \ldots, N+Z \tag{9}$$

where $a_{l\Lambda}^i$ and $a_{l\Lambda}^j$ are the coefficients of decomposition of the functions $v_i$ and $u_j$ in the basis of the spherical harmonic oscillator [11]; $N_i$ and $N_j$ are the principal quantum numbers of states $i$ and $j$; $l$ and $\Lambda$ are the angular momentum and its projection; $G_{E(M)\lambda}^{ij}$ correspond to the quantities $G_{E(M)\lambda}$ calculated in Ref. [11].

Note that the matrix element of the single-particle multipole operator is taken between two determinant wave functions. That is why the transition probabilities depend on the mixture coefficients $a_{l\Lambda}^i$ [Eqs. (8) and (9)] but not on any deformation parameters. Because the mixture coefficients are calculated numerically, it is not possible to derive analytical dependence of the transition probabilities on the deformation in the form of deformation parameters.

The case $\lambda \geq K + K'$ was studied in Ref. [15]. The influence of different deformations of the initial and final states of odd s-d-shell nuclei on the probabilities of $E2$-transitions was analyzed in Ref. [16]. The role of Coriolis interaction in calculations of the probabilities of electromagnetic transitions between states with different deformations was accounted for in Ref. [17]. The experimentally measured probabilities of $M1$-transitions between analogue and anti-analogue states with different deformations in odd s-d-shell nuclei were examined in Ref. [18].

Note that the authors of Refs. [12–18] restricted themselves to the case of quadrupole deformations. Using two different deformation parameters they plotted the area where the discrepancy between the measured and calculated probabilities of some $E2$-transitions for odd s-d-shell nuclei significantly reduced. But this was done numerically.

## 4. EVOLVING NUCLEAR SHAPES VIA EVOLUTIONARY ALGORITHM

We chose the function that describes the shape of the equipotential surface of the nuclear potential in the i-th single-particle state of the nucleus in the following form:

$$\varphi^{(i)}(\theta) = \sum_{k=0}^{\infty} \varphi_{2k}^{(i)} \cos(2k\theta). \tag{10}$$

The values of the weight parameters $\{\varphi_{2k}^{(i)}\}$ ($i=0$ marks the ground state and $i=1, \ldots, n$ mark the single-particle excited states) are determined independently for each level of the nucleus. Additional requirements imposed on the

weight parameters $\left\{\varphi_{2k}^{(i)}\right\}$ are their minimum number for each level and their minimum value that ensures a good description of experimental data. Note that both $\varepsilon$ and $\left\{\varphi_0^{(i)}\right\}$ affect the radius of spherical equipotential surface of the potential in the Hamiltonian (1). Thus, to avoid overestimation, we set $\left\{\varphi_0^{(0)}\right\}= 0$ .

To determine the number and values of the weight parameters $\left\{\varphi_{2k}^{(i)}\right\}$, an approach based on the use of an evolutionary algorithm [21,22] to fit the calculated observables to the measured ones was developed.

Our evolutionary approach operates on a population of $N$ individuals. Each individual is a set of parameters $\left(\varepsilon, \kappa, \left\{\varphi_{2k}^{(i)}\right\}\right)$, $i$=0, ..., $n$, $k$=0, ..., $m$. Fitness of each individual reflects the quality of data fitting provided by the individual's parameters. Using the mutation operation, the algorithm evolves the initial population of poorly fitted individuals to the final population of the well fitted ones.

Every iteration, the so-called generation, of our procedure contains the following steps.

1. Generating the initial population of $N$ individuals. For each individual, the values of all parameters $\left(\varepsilon, \kappa, \left\{\varphi_{2k}^{(i)}\right\}\right)$ are set to zero.

2. Evaluating fitness of each individual in the population. The fitness function accounts for the quality of data fitting, which is estimated using the standard $\chi^2$ magnitude per datum.

3. Letting each individual in the population produce $M$>>1 offspring. Replication of each parameter $x_j$ from the set $\left(\varepsilon, \kappa, \left\{\varphi_{2k}^{(i)}\right\}\right)$ is performed according to the transformation:

$$x_j' = x_j + A_j C_j , \tag{11}$$

$$A_j' = A_j \exp\left(L N_j (0,1)\right), \tag{12}$$

where $x_j$ and $x_j'$ are the parent's and the offspring's parameters from the set $\left(\varepsilon, \kappa, \left\{\varphi_{2k}^{(i)}\right\}\right)$, $A_j > 0$ and $A_j' > 0$ are the parent's and the offspring's mutation amplitudes, $A_j \in \left[A_{\min}; A_{\max}\right]$, $C_j$ is a Cauchy random variable with the scale parameter set to unity, $N_j(0,1)$ denotes a normally distributed one-dimensional random number with mean zero and one standard deviation, and $L > 0$ is the learning parameter that controls the adaptation speed.

4. Evaluating fitness values of all offspring. Sort offspring in descending order according to their fitness. Select $N$ best offspring to form the new population.

5. Going to step 3 or stop if the best fitness in the population is sufficiently high (the $\chi^2$ value is small enough).

The evolutionary process should produce the best possible solution with respect to the fitness function. To achieve this goal and avoid premature convergence in a local optimum, the lower limit of the mutation amplitude $A_{\min}$ behaves as a smooth oscillatory function of generation, while the upper limit $A_{\max}$ remains constant [remember that the real value of $A$ is adapted according to Eq.(12)]. If the value of $A_{\min}$ increases and the rms deviation from the mean value of the fitness function in the population exceeds some upper level (the diversity in the population is too high) then $A_{\min}$ starts to slowly decrease. And vice versa, if the value of $A_{\min}$ decreases and the rms deviation of the fitness function becomes less than some lower level (the diversity is too low) then $A_{\min}$ starts to slowly increase. However, before that, the best fitted individual is saved out of the converged population to preserve the globally best individual. Then, all individuals in the population jump to the new point in the parameter space according to the transformation:

$$x_j^* = x_j + a\left|x_j\right| C_j , \tag{13}$$

where $x_j$ and $x_j^*$ are the individual's parameters from the set $\left(\varepsilon, \kappa, \left\{\varphi_{2k}^{(i)}\right\}\right)$ before and after the jump, $C_j$ is a Cauchy random variable with the scale parameter set to unity, and $a \in \left[0;1\right]$ is the jump amplitude. Being transposed to the new point in the parameter space, the population starts to explore the vicinity of this point by increasing and decreasing $A_{\min}$ as described above. After finishing another cycle of evolution, the globally best individual is refreshed. Then the population is filled with the current globally best individual, next jump is performed, and new cycle of evolution begins.

Evolutionary algorithms make up, generally, the global optimization technique that, however, cannot guarantee that the optimum found is the global one (see, e.g., Refs. [23–25] or any textbook on evolutionary computations). Therefore, it is necessary to run the procedure several times. Besides, there is no way to know in advance what the minimum value of the $\chi^2$ magnitude will be. Thus, it is instructive to monitor the dynamics of the best, worst, and mean fitness values and the rms deviation from the mean fitness in the population during those several runs of the procedure in order to localize the region of the lowest $\chi^2$ values.

Analysis of experimental data begins with the assumption of the quadrupole deformation of the shapes of nucleus in the ground and single-particle excited states [the terms with $k$=0, 1 are left in Eq.(10)]. If the desired quality of data fitting is not

achieved within this assumption, then the hexadecapole deformation comes into play [the term with $k=2$ is added in Eq.(10)], and so forth. After the number of terms in Eq.(10) is determined, the contribution of the first term found (the term with $k=0$ that violates the volume conservation) is smoothly consistently reduced, preserving the desired quality of data fitting with that. If this procedure produces rather different solutions that are similar in fitness, the contribution of the term next to the previous one (say, $k=1$) is gradually reduced, and so forth. Following the described prescription, it appears possible to substantially reduce the parameter space of the problem under study and localize the region of the similar solutions.

The reason for the choice of deformation parameterization (10) is, to some extent, technological. The Hamiltonian (1) linearly depends on the function $\varphi(\theta)$. The radius of equipotential surface of the potential is $1/\sqrt{1-\varphi(\theta)}$. Thus, direct parameterization of the radius brings additional computational difficulties.

The decomposition (10) is analytically equivalent to the widely used decomposition of the radius of an axially symmetric nucleus into a series of spherical harmonics (see, e.g., Ref.[5]). Note that, e.g., the Legendre polynomial $P_4(\cos\theta)$ contains not only the term $\cos(4\theta)$, but also the term $\cos(2\theta)$ that is the kernel of the polynomial $P_2(\cos\theta)$. Thus, the decomposition of the function $\varphi(\theta)$ into the series of even Legendre polynomials gives, in fact, the term $\cos(2\theta)$ with two different free weight parameters. This makes additional difficulty for the search algorithm to determine these parameters. In other words, the decomposition (10) substantially simplifies the search for the solution of our problem. Besides, the decomposition (10) gives extremely concise description of the topological features of the nuclear shape.

After the parameters $\varphi_{2k}^{(i)}$ are determined, the values of conventional deformation parameters $\alpha_{2k}^{(i)}$ can be estimated using the following approximate correlation:

$$\frac{1}{\sqrt{1-\varphi^{(i)}(\theta)}} \approx 1+\frac{1}{2}\varphi^{(i)}(\theta)=1+\frac{1}{2}\sum_{k=0}^{m}\varphi_{2k}^{(i)}\cos(2k\theta)=1+\sum_{k=0}^{m}\alpha_{2k}^{(i)}P_{2k}(\cos\theta) \ . \tag{14}$$

## 5. $^{27}$Al NUCLEUS SHAPES IN LOW-LAYING SINGLE-PARTICLE STATES

Good quality of fit was achieved when the terms with $k=0, 1, 2$ were left in Eq.(10). The schemes of occupation of single-particle states by protons (proton configurations) in the ground (g.s.) and first three single-particle excited states (1–3 e.s.) of the $^{27}$Al nucleus were chosen as follows:

$$
\begin{array}{lccccccccccc}
\text{g.s.} & 2 & 2 & 2 & 2 & 2 & 2 & 1 & 0 & 0 & 0 & 0 \\
\text{1 e.s.} & 2 & 2 & 2 & 2 & 2 & 2 & 0 & 1 & 0 & 0 & 0 \\
\text{2 e.s.} & 2 & 2 & 2 & 2 & 2 & 2 & 0 & 0 & 0 & 1 & 0 \\
\text{3 e.s.} & 2 & 2 & 2 & 2 & 2 & 2 & 0 & 0 & 1 & 0 & 0
\end{array}
$$

The schemes of occupation of single-particle states by neutrons (neutron configurations) were chosen to be independent of the nucleus state:

$$
\begin{array}{cccccccccccc}
2 & 2 & 2 & 2 & 2 & 2 & 2 & 0 & 0 & 0 & 0
\end{array}
$$

Figure 1 and Tables 1–4 present the best fitted result. Experimental data were taken from Refs. [26,27].
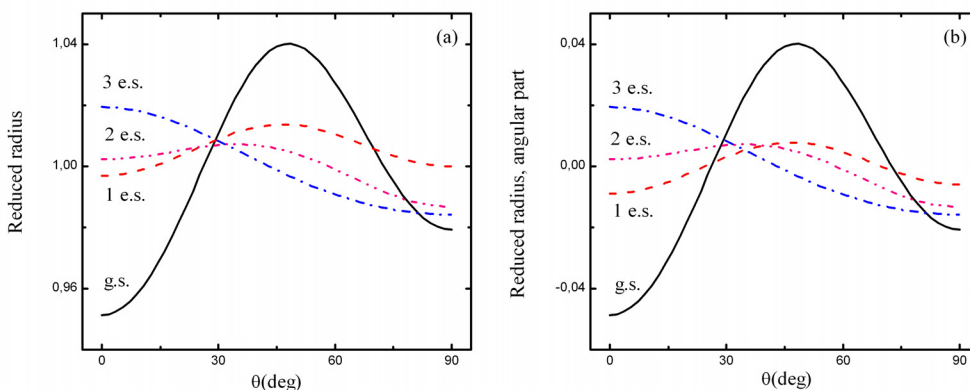


**Figure 1.** Shapes for four single-particle states of $^{27}$Al nucleus, calculated by our procedure. (a) Reduced radii $1/\sqrt{1-\varphi(\theta)}$ of the equipotential surface of the nuclear potential for four single-particle states of $^{27}$Al nucleus. (b) The same as Fig. 1(a) but only for angular part of $1/\sqrt{1-\varphi(\theta)}$. Curve marked as g.s. corresponds to the ground state. Curves marked as 1–3 e.s. present three low-laying excited states.

**Table 1.** Experimentally measured $E_{exper}(2J^\pi)$ and calculated $E_{theor}(2J^\pi)$ energies (MeV), spins $2J$, and parities $\pi$ of the ground and first three low-laying single-particle excited states of $^{27}$Al nuclei.

| $E_{exper}(2J^\pi)$ | $E_{theor}(2J^\pi)$ |
|---|---|
| 0.0000 (5$^+$) | 0.0000 (5$^+$) |
| 0.8438 (1$^+$) | 0.8438 (1$^+$) |
| 2.9820 (3$^+$) | 2.9820 (3$^+$) |
| 3.6804 (1$^+$) | 3.6804 (1$^+$) |

We are aware that the dynamics of nuclear deformation with the increase of excitation energy is better analyzed looking at the plot of the nuclear radius as function of the angle. Therefore, instead of the function $\varphi(\theta)$, we show the reduced radius of equipotential surface of the potential $1/\sqrt{1-\varphi(\theta)}$ [Fig. 1(a)] and its angular part $1/\sqrt{1-\varphi(\theta)}-1/\sqrt{1-\varphi_0}$ [Fig. 1(b)] as functions of the angle. Besides, Table 4 contains the values of conventional deformation parameters estimated with help of Eq. (14).

**Table 2.** Experimentally measured $\Gamma_{\gamma i}(E2)_{exper}$ and calculated $\Gamma_{\gamma i}(E2)_{theor}$ partial gamma widths (eV) for $^{27}$Al nuclei. $E_i(2J^\pi)$ and $E_f(2J^\pi)$ denote energies (MeV), spins 2J, and parities $\pi$ of initial and final states.

| $E_i(2J^\pi) \rightarrow E_f(2J^\pi)$ | $\Gamma_{\gamma i}(E2)_{exper}$ | $\Gamma_{\gamma i}(E2)_{theor}$ |
|---|---|---|
| 0.8438 (1$^+$) $\rightarrow$ 0.0000 (5$^+$) | $(1.30\pm0.20)\times10^{-5}$ | $1.30\times10^{-5}$ |
| 2.9820 (3$^+$) $\rightarrow$ 0.0000 (5$^+$) | $<4.55\times10^{-5}$ | $2.60\times10^{-5}$ |
| 3.6804 (1$^+$) $\rightarrow$ 0.0000 (5$^+$) | $(1.00\pm0.30)\times10^{-3}$ | $1.00\times10^{-3}$ |

**Table 3.** Experimentally measured $\Gamma_{\gamma i}(M1)_{exper}$ and calculated $\Gamma_{\gamma i}(M1)_{theor}$ partial gamma widths (eV) for $^{27}$Al nuclei. $E_i(2J^\pi)$ and $E_f(2J^\pi)$ denote energies (MeV), spins $2J$, and parities $\pi$ of initial and final states.

| $E_i(2J^\pi) \rightarrow E_f(2J^\pi)$ | $\Gamma_{\gamma i}(M1)_{exper}$ | $\Gamma_{\gamma i}(M1)_{theor}$ |
|---|---|---|
| 2.9820 (3$^+$) $\rightarrow$ 0.0000 (5$^+$) | $(1.14\pm0.03)\times10^{-1}$ | $1.14\times10^{-1}$ |
| 2.9820 (3$^+$) $\rightarrow$ 0.8438 (1$^+$) | $(1.20\pm0.40)\times10^{-3}$ | $1.20\times10^{-3}$ |
| 3.6804 (1$^+$) $\rightarrow$ 0.8438 (1$^+$) | $(5.20\pm0.20)\times10^{-2}$ | $5.20\times10^{-2}$ |

**Table 4.** Deformation parameters $\alpha_{2k}$, $k=0, 1, 2$, of the shape of $^{27}$Al nucleus in its ground (g.s.) and first three low-laying single-particle excited states (1–3 e.s.), estimated according to Eq. (14).

| | g.s. | 1 e.s. | 2 e.s. | 3 e.s. |
|---|---|---|---|---|
| $\alpha_0$ | $7.6\times10^{-3}$ | $6.8\times10^{-3}$ | $-2.2\times10^{-3}$ | $-5.9\times10^{-3}$ |
| $\alpha_2$ | $7.4\times10^{-3}$ | $3.6\times10^{-3}$ | $1.4\times10^{-2}$ | $2.2\times10^{-2}$ |
| $\alpha_4$ | $-6.7\times10^{-2}$ | $-1.3\times10^{-2}$ | $-1.0\times10^{-2}$ | $2.3\times10^{-3}$ |

Figure 1 and Table 4 show that the angular part of the $^{27}$Al nucleus shape is described by two harmonics – quadrupole [$\cos(2\theta)$ or $P_2(\cos\theta)$] and hexadecapole [$\cos(4\theta)$ or $P_4(\cos\theta)$]. In its ground and first three low-laying single-particle excited states the $^{27}$Al nucleus is abnormally weakly deformed. The hexadecapole deformation dominates in the ground state of the $^{27}$Al nucleus. Then, with the increase of the excitation energy, its contribution decreases and almost vanishes for the third excited state. The contribution of the quadrupole deformation is small for the ground and first excited states, but it increases with the increase of the excitation energy and becomes dominant for the third excited state of the $^{27}$Al nucleus.

## 6. $^{31}$P NUCLEUS SHAPES IN LOW-LAYING SINGLE-PARTICLE STATES

Good quality of fit was achieved when the terms with $k=0, 1, 2$ were left in Eq.(10). The schemes of occupation of single-particle states by protons (proton configurations) in the ground (g.s.) and first three single-particle excited states (1–3 e.s.) of the $^{31}$P nucleus were chosen as follows:

```
g.s.   2 2 2 2 2 2 2 1 0 0 0 0 0 0
1 e.s. 2 2 2 2 2 2 2 0 1 0 0 0 0 0
2 e.s. 2 2 2 2 2 2 1 2 0 0 0 0 0 0
3 e.s. 2 2 2 2 2 2 2 0 0 0 0 0 0 1
```

The schemes of occupation of single-particle states by neutrons (neutron configurations) were chosen to be independent of the nucleus state:

```
2 2 2 2 2 2 2 2 0 0 0
```

Figure 2 and Tables 5-9 present the best result. Experimental data were taken from Refs. [26,28].

As in Fig. 1, we show the reduced radius of equipotential surface of the potential [Fig. 2(a)] and its angular part [Fig. 2(b)] as function of the angle, while Table 9 contains the values of conventional deformation parameters estimated with help of Eq. (14).

**Table 5.** Experimentally measured $E_{\text{exper}}(2J^\pi)$ and calculated $E_{\text{theor}}(2J^\pi)$ energies (MeV), spins $2J$, and parities $\pi$ of the ground and first three low-laying single-particle excited states of $^{31}$P nuclei.

| $E_{\text{exper}}(2J^\pi)$ | $E_{\text{theor}}(2J^\pi)$ |
|---|---|
| 0.0000 (1$^+$) | 0.0000 (1$^+$) |
| 3.1343 (1$^+$) | 3.1343 (1$^+$) |
| 3.2950 (5$^+$) | 3.2950 (5$^+$) |
| 4.4312 (7$^-$) | 4.4312 (7$^-$) |

**Table 6.** Experimentally measured $\Gamma_{\gamma i}(E2)_{\text{exper}}$ and calculated $\Gamma_{\gamma i}(E2)_{\text{theor}}$ partial gamma widths (eV) for $^{31}$P nuclei. $E_{\text{i}}(2J^\pi)$ and $E_{\text{f}}(2J^\pi)$ denote energies (MeV), spins $2J$, and parities $\pi$ of initial and final states.

| $E_{\text{i}}(2J^\pi) \rightarrow E_{\text{f}}(2J^\pi)$ | $\Gamma_{\gamma i}(E2)_{\text{exper}}$ | $\Gamma_{\gamma i}(E2)_{\text{theor}}$ |
|---|---|---|
| 3.2950 (5$^+$) → 0.0000 (1$^+$) | (4.35±0.5)×10$^{-5}$ | 4.35×10$^{-5}$ |

**Table 7.** Experimentally measured $\Gamma_{\gamma i}(M1)_{\text{exper}}$ and calculated $\Gamma_{\gamma i}(M1)_{\text{theor}}$ partial gamma widths (eV) for $^{31}$P nuclei. $E_{\text{i}}(2J^\pi)$ and $E_{\text{f}}(2J^\pi)$ denote energies (MeV), spins $2J$, and parities $\pi$ of initial and final states.

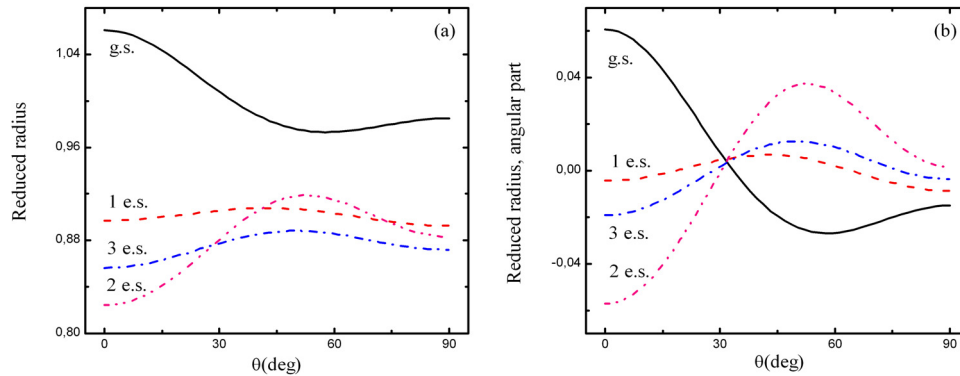| $E_{\text{i}}(2J^\pi) \rightarrow E_{\text{f}}(2J^\pi)$ | $\Gamma_{\gamma i}(M1)_{\text{exper}}$ | $\Gamma_{\gamma i}(M1)_{\text{theor}}$ |
|---|---|---|
| 3.1343 (1$^+$) → 0.0000 (1$^+$) | (6.2 ±0.5)×10$^{-2}$ | 6.2×10$^{-2}$ |



**Figure 2.** Shapes for four single-particle states of $^{31}$P nucleus, calculated by our procedure. (a) Reduced radii $1/\sqrt{1-\varphi(\theta)}$ of the equipotential surface of the nuclear potential for four single-particle states of $^{31}$P nucleus. (b) The same as Fig. 2(a) but only for angular part of $1/\sqrt{1-\varphi(\theta)}$. Curve marked as g.s. corresponds to the ground state. Curves marked as 1–3 e.s. present three low-laying excited states.

**Table 8.** Experimentally measured $\Gamma_{\gamma i}(E3)_{\text{exper}}$ and calculated $\Gamma_{\gamma i}(E3)_{\text{theor}}$ partial gamma widths (eV) for $^{31}$P nuclei. $E_{\text{i}}(2J^\pi)$ and $E_{\text{f}}(2J^\pi)$ denote energies (MeV), spins $2J$, and parities $\pi$ of initial and final states.

| $E_{\text{i}}(2J^\pi) \rightarrow E_{\text{f}}(2J^\pi)$ | $\Gamma_{\gamma i}(E3)_{\text{exper}}$ | $\Gamma_{\gamma i}(E3)_{\text{theor}}$ |
|---|---|---|
| 4.4312 (7$^-$) → 0.0000 (1$^+$) | (9.80±2.1)×10$^{-6}$ | 9.80×10$^{-6}$ |
| 4.4312 (7$^-$) → 3.1343 (1$^+$) | <1.10×10$^{-6}$ | 1.10×10$^{-6}$ |

**Table 9.** Deformation parameters $\alpha_{2k}$, $k = 0, 1, 2$, of the shape of $^{31}$P nucleus in its ground (g.s.) and first three low-laying single-particle excited states (1–3 e.s.), estimated according to Eq. (14).

|  | g.s. | 1 e.s. | 2 e.s. | 3 e.s. |
|---|---|---|---|---|
| $\alpha_0$ | -1.3×10$^{-2}$ | -1.1×10$^{-1}$ | -1.2×10$^{-1}$ | -1.4×10$^{-1}$ |
| $\alpha_2$ | 3.1×10$^{-2}$ | 1.0×10$^{-2}$ | -2.9×10$^{-2}$ | -2.6×10$^{-3}$ |
| $\alpha_4$ | 3.6×10$^{-2}$ | -1.6×10$^{-2}$ | -8.2×10$^{-2}$ | -3.1×10$^{-2}$ |

Figure 2 and Table 9 show that, as in case of $^{27}$Al nucleus, the angular part of the $^{31}$P nucleus shape is described by two harmonics – quadrupole and hexadecapole. In its ground and first three low-laying single-particle excited states the $^{31}$P nucleus is abnormally weakly deformed. The ground and first excited states of the $^{31}$P nucleus are characterized by the mixture of the quadrupole and hexadecapole deformations. Then, with the increase of the excitation energy, the hexadecapole deformation becomes dominant in the second and third excited states.

## 7. $^{35}$Cl NUCLEUS SHAPES IN LOW-LAYING SINGLE-PARTICLE STATES

Good quality of fit was achieved when the terms with $k=0, 1, 3$ were left in Eq.(10). The term $\cos(4\theta)$ ($k=2$) did not influence the quality of fit. The schemes of occupation of single-particle states by protons (proton

configurations) in the ground (g.s.) and first three single-particle excited states (1–3 e.s.) of the $^{35}$Cl nucleus were chosen as follows:

$$
\begin{array}{lcccccccccccccc}
\text{g.s.} & 2 & 2 & 2 & 2 & 2 & 2 & 2 & 2 & 1 & 0 & 0 & 0 & 0 & 0 \\
\text{1 e.s.} & 2 & 2 & 2 & 2 & 2 & 2 & 2 & 2 & 0 & 1 & 0 & 0 & 0 & 0 \\
\text{2 e.s.} & 2 & 2 & 2 & 2 & 2 & 2 & 2 & 2 & 0 & 0 & 0 & 0 & 0 & 1 \\
\text{3 e.s.} & 2 & 2 & 2 & 2 & 2 & 2 & 1 & 2 & 2 & 0 & 0 & 0 & 0 & 0
\end{array}
$$

The schemes of occupation of single-particle states by neutrons (neutron configurations) were chosen to be independent of the nucleus state:

$$
\begin{array}{ccccccccccc}
2 & 2 & 2 & 2 & 2 & 2 & 2 & 2 & 2 & 0 & 0
\end{array}
$$

Figure 3 and Tables 10-15 present the best result. Experimental data were taken from Refs. [26,29].

As in Figs. 1 and 2, we show the reduced radius of equipotential surface of the potential [Fig. 3(a)] and its angular part [Fig. 3(b)] as function of the angle, while Table 15 contains the values of conventional deformation parameters estimated with help of Eq. (14). We emphasized that in order to replicate well the experimental data on $^{35}$Cl nucleus it was not necessary to account for the contribution of the basis function $\cos(4\theta)$ in the decomposition (10). Thus, the values of the parameters $\varphi_4^{(i)}$ were set to zero and, consequently, the values of the deformation parameters $\alpha_4^{(i)}$ appeared to be linearly dependent on the values of the parameters $\alpha_6^{(i)}$ (Table 15).
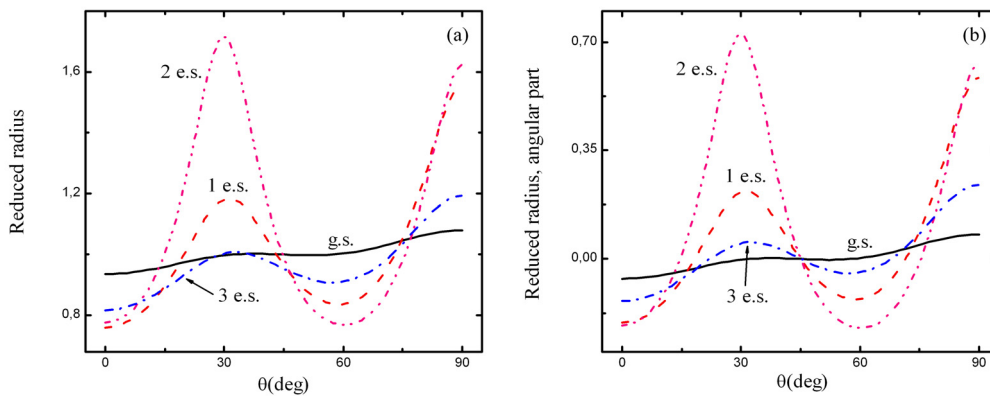


**Figure 3.** Shapes for four single-particle states of $^{35}$Cl nucleus, calculated by our procedure. (a) Reduced radii $1\big/\sqrt{1-\varphi(\theta)}$ of the equipotential surface of the nuclear potential for four single-particle states of $^{35}$Cl nucleus. (b) The same as Fig. 3(a) but only for angular part of $1\big/\sqrt{1-\varphi(\theta)}$. Curve marked as g.s. corresponds to the ground state. Curves marked as 1–3 e.s. present three low-laying excited states.

**Table 10.** Experimentally measured $E_{\text{exper}}(2J^\pi)$ and calculated $E_{\text{theor}}(2J^\pi)$ energies (MeV), spins $2J$, and parities $\pi$ of the ground and first three low-laying single-particle excited states of $^{35}$Cl nuclei.

| $E_{\text{exper}}(2J^\pi)$ | $E_{\text{theor}}(2J^\pi)$ |
|---|---|
| 0.0000 (3$^+$) | 0.0000 (3$^+$) |
| 1.2193 (1$^+$) | 1.2193 (1$^+$) |
| 3.1628 (7$^-$) | 3.1628 (7$^-$) |
| 3.9185 (3$^+$) | 3.9185 (3$^+$) |

**Table 11.** Experimentally measured $\Gamma_{\gamma i}(E2)_{\text{exper}}$ and calculated $\Gamma_{\gamma i}(E2)_{\text{theor}}$ partial gamma widths (eV) for $^{35}$Cl nuclei. $E_i(2J^\pi)$ and $E_f(2J^\pi)$ denote energies (MeV), spins $2J$, and parities $\pi$ of initial and final states.

| $E_i(2J^\pi) \rightarrow E_f(2J^\pi)$ | $\Gamma_{\gamma i}(E2)_{\text{exper}}$ | $\Gamma_{\gamma i}(E2)_{\text{theor}}$ |
|---|---|---|
| 1.2193 (1$^+$) → 0.0000 (3$^+$) | (4.0±0.44)×10$^{-5}$ | 4.0×10$^{-5}$ |
| 3.9185 (3$^+$) → 0.0000 (3$^+$) | (3.1±0.89)×10$^{-3}$ | 3.1×10$^{-3}$ |

**Table 12.** Experimentally measured $\Gamma_{\gamma i}(M1)_{\text{exper}}$ and calculated $\Gamma_{\gamma i}(M1)_{\text{theor}}$ partial gamma widths (eV) for $^{35}$Cl nuclei. $E_i(2J^\pi)$ and $E_f(2J^\pi)$ denote energies (MeV), spins $2J$, and parities $\pi$ of initial and final states.

| $E_i(2J^\pi) \rightarrow E_f(2J^\pi)$ | $\Gamma_{\gamma i}(M1)_{\text{exper}}$ | $\Gamma_{\gamma i}(M1)_{\text{theor}}$ |
|---|---|---|
| 1.2193 (1$^+$) → 0.0000 (3$^+$) | (3.6 ±0.4)×10$^{-3}$ | 3.6×10$^{-3}$ |
| 3.9185 (3$^+$) → 0.0000 (3$^+$) | (7.1 ±2.0)×10$^{-2}$ | 7.1×10$^{-2}$ |
| 3.9185 (3$^+$) → 1.2193 (1$^+$) | <5.0×10$^{-4}$ | 5.0×10$^{-4}$ |

**Table 13.** Experimentally measured $\Gamma_{\gamma i}(M2)_{exper}$ and calculated $\Gamma_{\gamma i}(M2)_{theor}$ partial gamma widths (eV) for $^{35}$Cl nuclei. $E_i(2J^\pi)$ and $E_f(2J^\pi)$ denote energies (MeV), spins $2J$, and parities $\pi$ of initial and final states.

| $E_i(2J^\pi) \rightarrow E_f(2J^\pi)$ | $\Gamma_{\gamma i}(M2)_{exper}$ | $\Gamma_{\gamma i}(M2)_{theor}$ |
|---|---|---|
| 3.1628 (7$^-$) → 0.0000 (3$^+$) | (1.3 ±0.03)×10$^{-5}$ | 1.3×10$^{-5}$ |

**Table 14.** Experimentally measured $\Gamma_{\gamma i}(E3)_{exper}$ and calculated $\Gamma_{\gamma i}(E3)_{theor}$ partial gamma widths (eV) for $^{35}$Cl nuclei. $E_i(2J^\pi)$ and $E_f(2J^\pi)$ denote energies (MeV), spins $2J$, and parities $\pi$ of initial and final states.

| $E_i(2J^\pi) \rightarrow E_f(2J^\pi)$ | $\Gamma_{\gamma i}(E3)_{exper}$ | $\Gamma_{\gamma i}(E3)_{theor}$ |
|---|---|---|
| 3.1628 (7$^-$) → 0.0000 (3$^+$) | (3.3±0.075)×10$^{-7}$ | 3.3×10$^{-7}$ |
| 3.1628 (7$^-$) → 1.2193 (1$^+$) | <3.0×10$^{-8}$ | 3.0×10$^{-8}$ |

**Table 15.** Deformation parameters $\alpha_{2k}$, $k$=0, 1, 2, 3, of the shape of $^{35}$Cl nucleus in its ground (g.s.) and first three low-laying single-particle excited states (1–3 e.s.), estimated according to Eq. (14). The values of the parameter $\alpha_4$ linearly depend on the values of the parameter $\alpha_6$.

| | g.s. | 1 e.s. | 2 e.s. | 3 e.s. |
|---|---|---|---|---|
| $\alpha_0$ | 1.6×10$^{-2}$ | 3.5×10$^{-3}$ | -4.4×10$^{-3}$ | -1.4×10$^{-2}$ |
| $\alpha_2$ | -6.1×10$^{-2}$ | -9.0×10$^{-2}$ | 8.1×10$^{-2}$ | -1.0×10$^{-1}$ |
| $\alpha_4$ | 2.1×10$^{-2}$ | 2.2×10$^{-1}$ | 3.3×10$^{-1}$ | 1.0×10$^{-1}$ |
| $\alpha_6$ | -4.8×10$^{-2}$ | -5.0×10$^{-1}$ | -7.3×10$^{-1}$ | -2.2×10$^{-1}$ |

Figure 3 and Table 15 show that the angular part of the $^{35}$Cl nucleus shape is described by three harmonics – quadrupole [ $P_2(\cos\theta)$ ], hexadecapole [ $P_4(\cos\theta)$ ], and hexacontatetrapole [ $P_6(\cos\theta)$ ]. Note again that, in case of $^{35}$Cl nucleus, the contribution of hexadecapole deformation is not independent. In its ground state the $^{35}$Cl nucleus is abnormally weakly deformed. With the increase of excitation energy, the contribution of hexacontatetrapole deformation sharply (by an order of magnitude) increases and becomes dominant for the first and third excited states, and especially for the second excited state. This observation indicates that the change of the state of the only one nucleon – the valence proton the spin and parity of which determine the spin and parity of the $^{35}$Cl nucleus – causes the shape phase transition from the high-symmetry phase – spherical ground state – to the low-symmetry phase – deformed excited states.

## 8. DISCUSSION

The evolutionary procedure of determining the shape of a nucleus in single-particle states presented in this article is aimed at searching for the globally optimal solution. However, being aware of the complexity of the problem under study and the fact that the actual number of fitting parameters is substantially greater than the actual number of data points, we do not expect to achieve it. Therefore, we consider the obtained results (Figs.1–3, and Tables 1–15) as very promising.

The shapes of the nuclei studied in the ground and low-laying single-particle excited states obtained in different runs of the procedure go rather close to each other. Besides, the variations of the parameter that takes into account the deviation of the energy scale from its simple estimate $\varepsilon$ and of the spin-orbit interaction strength $\kappa$ from run to run of the optimization procedure are found to be insignificant. This result is a consequence of application of the requirements imposed on the weight parameters $\left\{\varphi_{2k}^{(i)}\right\}$ from the decomposition (10). Namely, the number of these parameters must be the smallest possible for each level and the values of these parameters must be the smallest possible, ensuring a good description of experimental data along with that. From the formally mathematical viewpoint, these requirements are equivalent to the numerous constraints imposed on the variables $\left\{\varphi_{2k}^{(i)}\right\}$, which leads to the substantial reduction of the parameter space of the problem (the "effective" number of free parameters is much smaller than the "actual" one). One should also bear in mind that the measured probabilities of electromagnetic transitions between single-particle states of nuclei are the highly correlated data that are difficult to analyze. Thus, in this case, the belief that "anything can be fitted with a sufficient number of parameters", is a substantial oversimplification (see, e.g., Ref. [2]).

From the computational viewpoint, in general, the parameter space of our problem is highly dimensional, highly nonlinear, and has unknown and unpredictable topography. This makes the choice of an appropriate search method crucial. Evolutionary (or genetic) algorithms have many times proved very efficient in dealing with very difficult physical problems (see, e.g., Refs. [30–35]), so we have chosen it as a key element of our procedure. Usually, in evolutionary computations, the mutation amplitude is either constant, or decreases across the run of the evolutionary procedure. Often this leads the search algorithm in a local optimum in the parameter space. To avoid premature convergence in a local optimum, we have devised the special schedule of tuning the mutation amplitude, in which the latter behaves as a smooth oscillatory function of generation. This mechanism resembles, in part, the so-called "simulated annealing" approach to solve the optimization problems of combinatorial complexity. Due to the consecutive cycles of increasing and decreasing of the mutation amplitude, the population hops from the less fitted optimum to the more fitted one situated in the close vicinity. To have an opportunity to explore the parameter space much further, we

have allowed the population as a whole to periodically jump to the new point in the parameter space. As a consequence, we have managed to localize the region of the nuclear shapes that give the lowest values to the $\chi^2$ magnitude: Tables 1–15 show very good agreement between the calculated and measured observables.

In principle, our algorithm could treat $\varphi(\theta)$ as a numerical array and evolve it as a whole quantity with help of the diffused mutation operator devised in Refs. [21,22]. We emphasize that the devised approach of extracting nuclear shapes from the data does not depend on the particular nuclear data and the particular analytical tools (nuclear models) to analyze it. For instance, our approach, with minor changes, could be used to extract the matter-density distributions in nuclei [36], the radial dependence of the nuclear potentials [37], etc. from the suitable data. Our preliminary investigations show that our method enables to extract the radial dependence of the nuclear potentials from the set of energy levels. Thus, our method could be applied to the wide set of nuclear problems in wide mass region.

From the physics viewpoint, our analysis of experimental data on the energies, spins, and parities of the low-laying single-particle states and the probabilities of electromagnetic transitions between them in $^{27}$Al, $^{31}$P and $^{35}$Cl nuclei shows the following.

We have found that the studied nuclei in the ground states are abnormally weakly deformed, which is not expected for the nuclei in the shell middle. Even in their low-laying single-particle excited states, the nuclei $^{27}$Al and $^{31}$P are found to be weakly deformed, too. The change of the state of the only one nucleon – the valence proton the spin and parity of which determine the spin and parity of the $^{35}$Cl nucleus – causes the shape phase transition from the high-symmetry phase – spherical ground state – to the low-symmetry phase – deformed excited states. Hence, in case of $^{27}$Al, $^{31}$P and $^{35}$Cl nuclei, we are dealing with manifestation of the forces that are not related to the formation of nuclear shells.

The angular part of the $^{27}$Al and $^{31}$P nuclei shape is described by two harmonics – quadrupole and hexadecapole. The angular part of the $^{35}$Cl nucleus shape is described by three harmonics – quadrupole, hexadecapole, and hexacontatetrapole, but the contribution of hexadecapole deformation is not independent. It is usually assumed that quadrupole deformations are of the most importance, while hexadecapole deformations are good but rather small corrections to quadrupole deformations and may be important for describing the ground states of heavy nuclei (see, e.g., Refs. [1,2] or any textbook on nuclear physics). As for the higher multipolarity deformations, they are not considered to have much physical significance. At present, there are no fundamental nuclear models that account for or predict the dominant hexacontatetrapole deformation, especially for light and medium nuclei.

Analyzing quantum characteristics of the single nucleons that form the $^{27}$Al, $^{31}$P and $^{35}$Cl nuclei, we find that the spin and parity of these nuclei are determined by the spin and parity of the last odd (valence) proton. At the same time, some of the nucleons of the nucleus core change their characteristics, too. This means that the electromagnetic transitions between the single-particle states of the $^{27}$Al, $^{31}$P and $^{35}$Cl nuclei are the multi-particle processes.

Applications of the Landau theory of phase transitions, briefly mentioned in the Introduction, are based on the decomposition of the radius of a nucleus, which depends on spherical angles, into a series of spherical functions [5]. Thus, the potential energy of the nucleus contains collective forces that act on the deformation parameters, but not on the angular variables. Strictly speaking, to predict the equilibrium shape of the nucleus, the theory must contain angular derivatives of various orders.

Spatial derivatives naturally arise in the Landau-type theory of phase transitions with a spatially inhomogeneous order parameter (see, e.g., Ref. [38] or any textbook on phase transitions). This theory turned out to be very effective in describing phase transitions in ferroelectrics and magnetics with incommensurate phases (see, e.g., Refs. [39–42] and also Ref. [33]). These phases are states in which the period of spatial modulation of the order parameter is not commensurate with (or does not depend on) the period of the crystal lattice. In this case, the Landau-type potential is a functional of the order parameter and its derivatives. The competition and compromise of different powers of the order parameter and its derivatives lead to the appearance of various stable spatially inhomogeneous states of the system.

Assuming that the characteristic size at which the angular function describing the deviation of the nucleus shape from sphericity changes significantly is not commensurate with both the size of the nucleon and the distance between the nucleons, the deformed nucleus can be considered as an incommensurate phase. Therefore, the Landau-type theory of phase transitions with a spatially inhomogeneous order parameter could be a useful tool to study the shape of a deformed nucleus.

**ORCID**
⬤**Volodymyr Yu. Korda,** https://orcid.org/0000-0002-9445-0461, ⬤**Iryna S. Timchenko**, https://orcid.org/0000-0003-2917-5026

**REFERENCES**
[1]  M.A. Preston, and R.K. Bhaduri, *Structure of the Nucleus* (Addison-Wesley, Reading, MA, 1975), 716 p.
[2]  W. Greiner, and J. Maruhn, *Nuclear Models* (Springer, Berlin, 1996), 376 p.
[3]  L. Landau, Phys. Z. Sowjet. **11**, 545 (1937). In *Collected Papers of L. D. Landau*, edited by D. Ter Haar (Pergamon, Oxford, 1965), p. 193.
[4]  P. Cejnar, J. Jolie, and R.F. Casten, Rev. Mod. Phys. **82**, 2155 (2010). https://doi.org/10.1103/RevModPhys.82.2155
[5]  A. Bohr, and B. Mottelson, *Nuclear Structure*, Vol. 2, (Benjamin, Reading, MA, 1975).
[6]  R. Lucas, Europhysics News, **32**, 5 (2001); http://dx.doi.org/10.1051/epn:2001101
[7]  D. Warner, Nature, **420**, 614 (2002). https://www.nature.com/articles/420614a
[8]  R.F. Casten, Nature Physics, **2**, 811 (2006). https://www.nature.com/articles/nphys451
[9]  S. Quan, Z.P. Li, D. Vretenar, and J. Meng, Phys. Rev. C, **97**, 031301(R) (2018). https://doi.org/10.1103/PhysRevC.97.031301

[10] M.T. Mustonen, C.N. Gilbreth, Y. Alhassid, and G.F. Bertsch, Phys. Rev. C **98**, 034317 (2018). https://doi.org/10.1103/PhysRevC.98.034317

[11] S.G. Nilsson, "Binding States of Individual Nucleos in Strongly Deformed Nuclei," Mat. Fys. Medd. **29**(16), 1-68 (1955). https://cds.cern.ch/record/212345/files/p1.pdf

[12] E.V. Inopin, E.G. Kopanets, L.P. Korda, V.Ya. Kostin, and A.A. Koval, Voprosy Atomnoi Nauki i Tekhniki, Seriya: Fizika Vysokih Energii i Atomnogo Yadra [Problems of Atomic Science and Technology, Series "Physics of High Energies and Atomic Nucleus"], **3**(15), 31 (1975) (in Russian). https://inis.iaea.org/search/searchsinglerecord.aspx?recordsFor=SingleRecord&RN=9361989

[13] E.G. Kopanets, E.V. Inopin, and L.P. Korda, Izv. Akad. Nauk SSSR, Ser. Fiz. [Bull. Acad. Sci. USSR, Phys. Ser.] **39**, 2032 (1975) (in Russian).

[14] E.G. Kopanets, E.V. Inopin, L.P. Korda, V.A. Kostin, and A.A. Koval, Izv. Akad. Nauk SSSR, Ser. Fiz. [Bull. Acad. Sci. USSR, Phys. Ser.] **40**, 780 (1976) (in Russian).

[15] E.G. Kopanets, E.V. Inopin, and L.P. Korda, Izv. Akad. Nauk SSSR, Ser. Fiz. [Bull. Acad. Sci. USSR, Phys. Ser.] **44**, 1947 (1980) (in Russian). https://www.osti.gov/etdeweb/biblio/5791741

[16] L.P. Korda, and E.G. Kopanets, Voprosy Atomnoi Nauki i Tekhniki, Seriya: Obshchaya I Yadernaya Fizika [Problems of Atomic Science and Technology, Series "General and Nuclear Physics"], **2**(16), 3 (1981) (in Russian).

[17] L.P. Korda, E.G. Kopanets, and E.V. Inopin, Voprosy Atomnoi Nauki i Tekhniki, Seriya: "Obshchaya i Yadernaya Fizika" [Problems of Atomic Science and Technology, Series "General and Nuclear Physics"], **2**(27), 63 (1984) (in Russian).

[18] A.N. Vodin, E.G. Kopanets, L.P. Korda, and V.Yu. Korda, Problems of Atomic Science and Technology, Series "Nuclear Physics Investigations", **2**(41), 66 (2003). https://vant.kipt.kharkov.ua/TABFRAME1.html

[19] V.Yu. Korda, I.S. Timchenko, L.P. Korda, O.S. Deiev, and V.F. Klepikov, Nucl. Phys. **A1025**, 122480 (2022). https://doi.org/10.1016/j.nuclphysa.2022.122480

[20] H.A. Bethe, *Intermediate Quantum Mechanics* (Benjamin, New York, 1964), 416 p.

[21] V.Yu. Korda, A.S. Molev, and L.P. Korda, Phys. Rev. C, **72**, 014611 (2005). https://doi.org/10.1103/PhysRevC.72.014611

[22] V.Yu. Korda, S.V. Berezovsky, A.S. Molev, and V.F. Klepikov, Int. J. Mod. Phys. C, **24**, 1350009 (2013). https://doi.org/10.1142/S0129183113500095

[23] J.H. Holland, *Adaptation in Natural and Artificial Systems* (The University of Michigan Press, Ann Arbor, 1975).

[24] D.E. Goldberg, *Genetic Algorithms in Search, Optimization and Machine Learning* (Addison-Wesley, 1989).

[25] Z. Michalewicz, *Genetic Algorithms + Data Structures = Evolution Programs* (Springer-Verlag, Berlin, 1994).

[26] P.M. Endt, Nucl. Phys. **A633**, 1 (1998). https://doi.org/10.1016/S0375-9474(97)00613-1

[27] M.S. Basunia, Nucl. Data Sheets, **112**, 1875 (2011). https://doi.org/10.1016/j.nds.2011.08.001

[28] C. Ouelet, and B. Singh, Nucl. Data Sheets, **114**, 209 (2013). https://doi.org/10.1016/j.nds.2013.03.001

[29] J. Chen, J. Cameron, and B. Singh, Nucl. Data Sheets, **112**, 2715 (2011). https://doi.org/10.1016/j.nds.2011.10.001

[30] J.R. Morris, D.M. Deaven, and K.M. Ho, Phys. Rev. B, **53**, R1740 (1996). https://doi.org/10.1103/PhysRevB.53.R1740

[31] K. Michaelian, Revista Mexicana de Fisica. **42**, 203 (1996).

[32] C. Winkler, and H.M. Hofmann, Phys. Rev. C, **55**, 684 (1997). https://doi.org/10.1103/PhysRevC.55.684

[33] S.V. Berezovsky, V.Yu. Korda, and V.F. Klepikov, Phys. Rev. B, **64**, 064103 (2001). https://doi.org/10.1103/PhysRevB.64.064103

[34] V.Yu. Korda, A.S. Molev, V.F. Klepikov, and L.P. Korda, Phys. Rev. C, **91**, 024619 (2015). https://doi.org/10.1103/PhysRevC.91.024619

[35] V.Yu. Korda, A.S. Molev, L.P. Korda, and V.F. Klepikov, Phys. Rev. C, **97**, 034606 (2018). https://doi.org/10.1103/PhysRevC.97.034606

[36] Yu.A. Berezhnoy, V.Yu. Korda, and A.G. Gakh, Int. J. of Mod. Phys. E, **14**, 1073 (2005). https://doi.org/10.1142/S0218301305003697

[37] V.Yu. Korda, Int. J. of Mod. Phys. E, **9**, 449 (2000). https://doi.org/10.1142/S0218301300000349

[38] J.C. Tolédano, and P. Tolédano, *The Landau Theory of Phase Transitions* (World Scientific, Singapore, 1987), 472 p.

[39] R.M. Hornreich, M. Luban, and S. Shtrikman, Phys. Rev. Lett. **35**, 1678 (1975). https://doi.org/10.1103/PhysRevLett.35.1678

[40] Y. Ishibashi, and H. Shiba, J. Phys. Soc. Jpn. **45**, 409 (1978). https://doi.org/10.1143/JPSJ.45.409

[41] V. Berezovsky, V.F. Klepikov, V.Yu. Korda, and N.A. Shlyakhov, Int. J. of Mod. Phys. B, **12**, 433 (1998). https://doi.org/10.1142/S0217979298000284

[42] H.Z. Cummins, Phys. Rep. **185**, 211 (1990). https://doi.org/10.1016/0370-1573(90)90058-A

## ДЕФОРМАЦІЯ НЕПАРНИХ ЯДЕР $^{27}$Al, $^{31}$P ТА $^{35}$Cl В ОДНОЧАСТИНКОВИХ СТАНАХ
**Володимир Ю. Корда[a], Лариса П. Корда[b], В'ячеслав Ф. Клепіков[a], Ірина С. Тімченко[b]**

*[a]Інститут електрофізики і радіаційних технологій, Національна академія наук, Харків, Україна*
*[b]Національний науковий центр "Харківський фізико-технічний інститут", Національна академія наук, Харків, Україна*

Форми непарних ядер s-d-оболонки $^{27}$Al, $^{31}$P та $^{35}$Cl в основних і одночастинкових збуджених станах вилучені з експериментальних даних про енергії, спіни та парності цих станів, а також виміряні імовірності електромагнітних переходів між ними за допомогою недавно розробленого нами еволюційного підходу. Ключовим елементом нашої процедури є еволюційний алгоритм, який приводить популяцію ядерних форм, що погано описують експериментальні дані, до популяції ядерних форм, що добре описують експериментальні дані. Досліджені ядра в їхніх основних станах виявились аномально слабко деформованими, що не притаманно ядрам в середині оболонки. Навіть в їхніх низько лежачих одночастинкових станах ядра $^{27}$Al та $^{31}$P виявились теж слабко деформованими. Із зростанням одночастинкової енергії збудження зміна стану єдиного нуклона – валентного протона, спін та парність якого визначають спін та парність ядра $^{35}$Cl – викликає фазовий перехід із високо симетричної фази – сферичного основного стану – у низько симетричну фазу – деформовані збуджені стани. Кутова частина форми ядер $^{27}$Al та $^{31}$P описується двома гармоніками – квадрупольною і гексадекапольною. Кутова частина форми ядра $^{35}$Cl описується трьома гармоніками – квадрупольною, гексадекапольною і гексаконтатетрапольною, проте внесок гексадекапольної деформації не є незалежним. В теперішній час немає фундаментальної ядерної моделі яка б враховувала або передбачала домінуючу гексаконтатетрапольну деформацію, особливо для легких і середніх ядер. Ми знайшли, що спін та парність ядер $^{27}$Al, $^{31}$P та $^{35}$Cl визначаються спіном та парністю останнього непарного протона. В той же час деякі нуклони остову ядра теж змінюють свої характеристики. Тому електромагнітні переходи між одночастинковими станами ядер $^{27}$Al, $^{31}$P та $^{35}$Cl є багаточастинковими процесами.

**Ключові слова:** *ядерна деформація; модель деформованих оболонок; одночастинковий стан; ядра s-d-оболонки; еволюційний алгоритм; фазовий перехід*